

See discussions, stats, and author profiles for this publication at: <https://www.researchgate.net/publication/274898983>

# Toward the Design of Highly Stable Small Colloidal SERS Substrates with Supramolecular Host–Guest Interactions for Ultrasensitive Detection

ARTICLE *in* THE JOURNAL OF PHYSICAL CHEMISTRY C · APRIL 2015

Impact Factor: 4.77 · DOI: 10.1021/acs.jpcc.5b01647

---

CITATIONS

3

READS

49

## 5 AUTHORS, INCLUDING:



Juan C. Fraire

National University of Cordoba, Argentina

9 PUBLICATIONS 46 CITATIONS

[SEE PROFILE](#)



Eduardo Andres Coronado

National University of Cordoba, Argentina

60 PUBLICATIONS 5,332 CITATIONS

[SEE PROFILE](#)

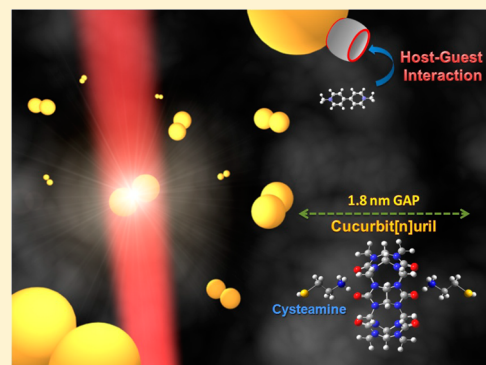
# Toward the Design of Highly Stable Small Colloidal SERS Substrates with Supramolecular Host–Guest Interactions for Ultrasensitive Detection

Juan C. Fraire,<sup>†</sup> Valeria N. Sueldo Ocello,<sup>‡</sup> Leandro G. Allende,<sup>†</sup> Alicia V. Veglia,<sup>‡</sup> and Eduardo A. Coronado<sup>\*,†</sup>

<sup>†</sup>INFIQC, Centro Laser de Ciencias Moleculares, Departamento de Fisicoquímica, and <sup>‡</sup>INFIQC, Departamento de Química Orgánica, Facultad de Ciencias Químicas, Universidad Nacional de Córdoba, Córdoba, 5000, Argentina

## S Supporting Information

**ABSTRACT:** In this work, we report a simple strategy to obtain ultrasensitive SERS nanostructures by self-assembly of Au nanospheres (NSs). This novel protocol allows us to obtain in a reproducible manner Au NS dimers using cucurbit[6]uril (CB[6]) molecules as linkers. The resulting dimers are stable in colloidal dispersion over several days, generating in this way nanostructures with highly reproducible hot spots. This feature is due to the precise subnanometric control of the molecules that generates interparticle distance and, at the same time, of the capability of placing analyte molecules just within these junctions of ultrahigh field enhancement due to the host–guest properties of the CB[6] molecule. The dimer formation is based on the modification of the metal surface with cysteamine molecules (Cys) previous incubation with CB[6] molecules. The cysteamine-functionalized NSs (Cys/NSs) are positive charged due to the protonation of the amine groups of the Cys molecule at the working pH. These positive groups interact through H-bonds with the carbonyl groups at the portal of the CB[6] molecules. The dimer formation is based on the stoichiometric control between Cys/NPs and CB[6] (ratio 2:1), generating a gap of 1.8 nm and giving rise to SERS enhancements of around  $10^8$ . The host–guest properties of the CB[6] molecule are used to detect the average SERS enhancement produced by adding methyl viologen (MV) as plasmonic probe. It was found that the average analytical enhancement factor (AEF) for MV is as good as that obtained for the CB[6] itself (around  $10^8$ ).



## INTRODUCTION

Noble metal nanoparticles (NPs) are well-known to exhibit a strong interaction with light determined by coherent collective electron oscillations, the so-called localized surface plasmon resonances (LSPR), which induce an enhanced electromagnetic field surrounding the metallic nanostructure with a spatial distribution that depends on their geometry, their orientation with respect to the incident polarization, illumination wavelength, and dielectric environment.<sup>1</sup> On resonance, the plasmon oscillation gives rise to a strongly enhanced electric field at the NP surface<sup>2</sup> and to a strongly enhanced scattering pattern in the far-field.<sup>2</sup> In addition, the LSPR frequencies can be tuned changing geometrical parameters, such as NP size,<sup>1</sup> shape,<sup>1</sup> crystal face and surface roughness,<sup>3,4</sup> and interparticle spacing.<sup>5–10</sup> In that sense, if two or more NPs approach each other to within approximately one particle diameter, the oscillating E-fields surrounding the NPs interfere and induce a coupling of the plasmon modes of the individual NPs.<sup>2,11,12</sup> This coupling gives rise to the so-called hot spots generated within the NP gaps (calculations of the field strengths in the coupling region between adjacent NPs typically reveal that interparticle fields can be many orders of magnitude greater

than the fields at the surface of single NPs).<sup>7–9</sup> The strong interactions of plasmons in coupled-NP can render possible many useful applications including surface enhanced Raman spectroscopy (SERS) bio(nano)sensors<sup>13,14</sup> and also NP waveguides.<sup>10</sup> In particular, SERS is a highly sensitive, simple (negligible sample preparation) and fast molecular fingerprinting technique.

Nowadays, the synthesis and fabrication of SERS substrates have evolved considerably due to the current capability of controlling the interparticle spacing by varying the specific particle functionalization. This is a very interesting and challenging research topic as gap distances play a key role in the surface-enhancing properties of NP assemblies (i.e., it determines the magnitude of enhanced field within the hot spot).<sup>15–17</sup> In this respect, one of the main aspects to consider in order to fabricate NP SERS substrates is to create structures with uniform hot spots. There are two commonly used strategies to generate controlled NP assemblies: The first one

Received: February 17, 2015

Revised: April 1, 2015

involves the use of biomolecules, which have the capability of being specific linkers and also biorecognition agents that serve to construct nanoscale architectures with precise control of the geometrical position of the NPs in the final nanostructure.<sup>18</sup> The second one is based on the use of organic molecules as molecular linkers to generate the self-assembly of metal NPs. The second strategy, particularly leads to smaller gaps (subnanometer gaps) between linked NPs than when biomolecules are used as linkers. Nevertheless, there is less control on the final nanostructure arquitecture, and it generally leads to randomly distributed particles in the final nanostructure.<sup>18</sup>

Besides the critical need to generate SERS substrates through NP assembly with small and uniform gaps between NPs and with precise control of the geometrical position of the NPs, there is another important issue that should also be taken into account: placing the analyte molecules precisely in the hot spot. In this respect, the Scherman group recently has proposed a new strategy involving the use of rigid barrel-shaped molecules (cucurbit[n]uril molecules, CB[n]) with host–guest interactions. This approach not only generates reproducible subnanometer interparticle distances, but also allows to localize the analyte molecule within the hot spot.<sup>19–24</sup> Cucurbit[n]urils are rigid and highly symmetric macrocycles with supramolecular host properties, synthesized by an acid-catalyzed condensation between glycoluril and formaldehyde.<sup>25</sup> The skeleton of C and N atoms defines a highly rigid and symmetric cavity with a hydrophobic inner cavity that could act as a potential inclusion site, whereas both portals are identical and surrounded by carbonyl groups, allowing ion-dipole or hydrogen bond interactions.<sup>26,27</sup> These properties characterize CB[n] as a family of promising molecular hosts that have the potential to be applied for the detection of a variety of chemical species, such as cations,<sup>28</sup> radical cations,<sup>29,30</sup> anions,<sup>31</sup> and neutral molecules.<sup>25,32</sup>

There are several works that have applied these properties of CB[n] molecules as NP self-assembly linkers,<sup>20,21</sup> and have used this CB[n]-assembled NP aggregates as SERS substrates for sensing applications.<sup>23,24</sup> In that sense, Scherman group has made a lot of effort in order to rationalize the optical response of the resulting nanostructure during the aggregation process. The work by Jones et al. present significant advances in controlling the aggregation of Au NPs (in particular, using Au nanorods) with small inter-rod separations, but there is still no control of the orientation of the aligned rods, which affects the interparticle plasmon coupling and, in that sense, affects the SERS enhancement that could be achieved.<sup>33</sup> It is well-known that the optical properties of the nanostructures could change dramatically during the aggregation and for a given NP size and gap separation, and this variation depends strongly on the irradiation wavelength and the nature of the metal.<sup>30</sup> Under these conditions, the gaps can be uniformly regulated by the rigid linker, but certainly the SERS enhancements produced should not be equivalent in each hot spot within the NP aggregate, since each of them could be coupled to a different dielectric environment (number of NPs and their geometrical arrangement around the hot spot). This feature may produce complex interference of the several multipole plasmon modes giving rise to lower enhancements than in nanostructures with a more controlled geometry (i.e., NP dimers).<sup>34</sup>

In this work, we report a simple synthetic strategy to obtain SERS dimeric structures by self-assembly of Au NS in which the SERS-active region (i.e., the gap between the NPs) consists

of metal-cysteamine-CB[n]-cysteamine-metal junctions. In this gap, the CB[n] molecule acts as the SERS reporter and it is localized in the region of maximum enhancement of the hot spot. This issue has an important implication since by means of the host–guest interactions it is possible to precisely localize a suitable analyte molecule in this region. The dimeric structures were generated using a stoichiometric control between the number of CB[n] molecules and the number of cysteamine-functionalized NSs (Cys/NSs) taking into account the fact that each CB[n] molecule can interact with a maximum of two functionalized NSs.

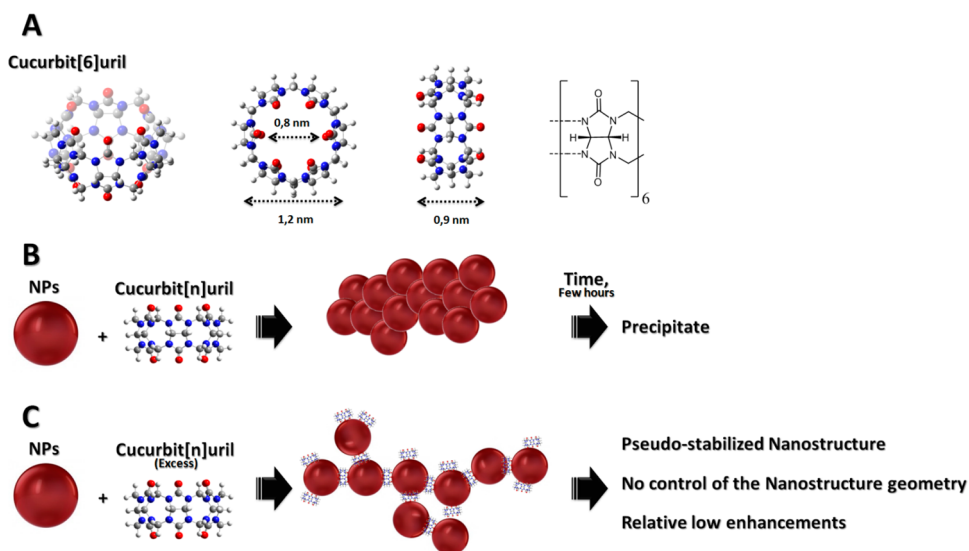
Using this strategy we have produced stable NS dimers, which is one of the most efficient and widely used configurations in studies involving SERS phenomena, using the carbonyl portals of the CB[n] molecule through the H-bond interactions with the protonated amine group of the cysteamine molecules adsorbed onto the NSs. The central improvement here over previous works involving CB[n]-assembled NP aggregates is the development and design of an optimized NP linking protocol in which the SERS signal itself is used as the optimization parameter. This leads to a SERS substrate in aqueous phase with an unprecedented SERS intensity and reproducibility which combines the best characteristics of the biomolecule-assisted assembly strategy (precise control of the nanostructure geometry) and the special characteristics of CB[n] molecules (uniformly spaced and smaller gaps, and capability to produce host–guest interactions to precise localization of the analyte molecule in the hot spots). The result is a quasi-isolatable, surface-functionalized material with uniform Raman response that can be generated in reproducible manner and that are stable in colloidal solution for several days. In particular we used the 6 unit homologue, cucurbit[6]uril (CB[6]) as it is one of the most difficult homologues to work with due to its very low solubility in aqueous media and the small portal gap.<sup>25</sup> Nevertheless, we believe that this synthetic strategy can be easily extrapolated with no further complications to the other homologues (CB[7] and CB[8]) spreading the application to the SERS ultrasensitive detection of more than one guest molecule due to the biggest diameter of the CB[n] nanocavity.<sup>23,24</sup>

## MATERIALS AND METHODS

**Materials.** The following materials were used as obtained: HAuCl<sub>4</sub> (Carlo Erba); Sodium Citrate (Mallinckrodt); Ascorbic Acid (Anedra); Cysteamine (Aldrich); Glycoluril (Aldrich); Formaldehyde Solution (36% in water, Fluka); Hydrochloric acid was of analytical grade (Cicarelli); Methyl Viologen (Aldrich).

**Au Nanospheres Synthesis.** The synthesis of gold NPs was performed using the Turkevich method,<sup>35</sup> which is based on the reduction properties of boiling citrate solutions. Briefly, they were produced by reducing a 50 mL 0.2 mM chloroauric acid solution (HAuCl<sub>4</sub>) with the addition of 0.5 mL of a 0.01 M citrate solution (corresponding to a 1:0.5 Au/citrate molar ratio) under heat and rapid stirring for 30 min. The morphological characterization of the Au NSs was performed combining UV-vis spectroscopy, TEM, and electrodynamic modeling using Mie theory. The overall results after combining all of these different techniques and modeling indicate that the average diameter of Au NSs was 76 nm with a concentration of  $8.01 \times 10^{10}$  NSs/cm<sup>3</sup> ( $1.33 \times 10^{-10}$  M), estimated using the experimental extinction intensities at the maximum wavelength, and the cross section calculated using Mie theory for spherical

**Scheme 1.** Synthetic Scheme Showing the Current Nanogap Engineering for the Generation of Nanospheres Aggregates with Cucurbit[n]uril<sup>a</sup>



<sup>a</sup>(A) Geometrical parameters of the cucurbit[6]uril molecule. Current strategies to generate of Au NSs assemblies. (B) Mixing comparable amounts of cucurbit[n]uril molecules and Au NSs leads to an uncontrollable interparticle spacing and finally to NSs precipitation. (C) Using a high cucurbit[n]uril excess leads to more stabilized nanostructures but with poor SERS performance.

particles with the suitable average diameter (determined by TEM).

**Particle Functionalization.** Cysteamine was used for the surface modification of 76 nm Au NSs. The procedure consist in incubating the colloidal dispersion using simultaneously cysteamine and ascorbic acid (which acts as reducing agent breaking the disulfide bonds between cysteamine molecules) around 2 h at room temperature. The amount of cysteamine was high enough to guarantee a completely surface functionalization of the Au NSs (cysteamine concentration:  $1 \times 10^{-6}$  M). The cysteamine-functionalized NSs (Cys/NSs) were washed by centrifugation (2268 rcf, 10 min) and resuspended in water.

For the generation of dimeric structures, 30 mL NS solution was incubated simultaneously with CB[6] molecules (molar ratio between Cys/NSs and CB[6] 2:1) for 30 min at room temperature.

**Extinction Measurements.** The characterization by UV-vis spectroscopy was carried out scanning in the 300–1100 nm range. The spectra were measured using a Shimadzu UV-1700 PharmaSpec spectrophotometer with a 1 cm quartz cell at room temperature.

**Zeta-Potential Measurements.** Zeta-potential measurements of citrate stabilized NSs and cysteamine functionalized NSs (Cys/NSs) were performed using a Delsa Nano 2.2 spectrometer at room temperature.

**Transmission Electron Microscopy.** Transmission electron microscopy (TEM) images were obtained using a JEM-JEOL 1120 EXII under an accelerating voltage of 80 kV. Samples were prepared by adding one drop ( $\sim 50 \mu\text{L}$ ) of the samples colloidal solution onto a holey carbon-Formvar coated copper TEM grid (100 mesh).

**Cucurbit[6]uril Synthesis.** Cucurbit[6]uril was synthesized from glycoluril and formaldehyde according to the method described in the literature,<sup>36</sup> implementing modifications in the separation and purification process.<sup>37</sup> CB[6] solutions were

prepared acidic media (HCl 18%, w/v) as it is necessary for its solubilization.

**SERS Measurements.** SERS measurements were performed using a Horiba LabRaman confocal microscope with a 100× (NA = 0.70) objective in the backscattering geometry. The spectra acquisition time was 20 s with a 600 lines  $\text{mm}^{-1}$  grating, giving a resolution of 4  $\text{cm}^{-1}$ . The excitation wavelength used was 633 nm (laser line from He-Ne). All measurements were performed at room temperature and were calibrated to Si and to  $\text{H}_2\text{O}$  bands in the colloidal solutions.

**Computational Methods.** The optical response of Au NSs were computed using the Generalized Multiparticle Mie Theory (GMM), as described elsewhere.<sup>38–40</sup> In all near field calculations presented in this work, the dielectric function tabulated by Palik for Au was employed.<sup>41</sup> For the GMM calculations of the cluster near field optical properties, a multipolar expansion order of 25 was used. In all the calculations performed in this work, the NPs were excited by a plane wave with an incidence pointing vector (propagation direction) normal to the surface. The angular average enhancement factor denoted by  $\langle \Gamma \rangle_\theta$  has been computed, averaged over 18 different polarizations (from 0° to 170° at 10° steps).

**Quantum Chemistry Calculations.** Ab initio calculations were performed with the Gaussian 98 program suite.<sup>42</sup> In all calculations, we use Becke's three-parameter hybrid functional method using Lee-Yang-Parr correlation functional (B3LYP) methods with 6-311++G(d,p) basis sets.

## RESULTS AND DISCUSSION

**Formation of Random Aggregates: Cucurbit[6]uril Self-Assembled NSs.** In this section we are going to discuss the general properties of random aggregates generated by direct assembly with CB[6] molecules. CB[6] is a six glycoluril unit macrocycle with the following structural parameters (Scheme 1A): portal diameter, 0.39 nm; cavity diameter, 0.58 nm; cavity volume, 164  $\text{\AA}^3$ ; outer diameter, 1.44 nm; and height, 0.91

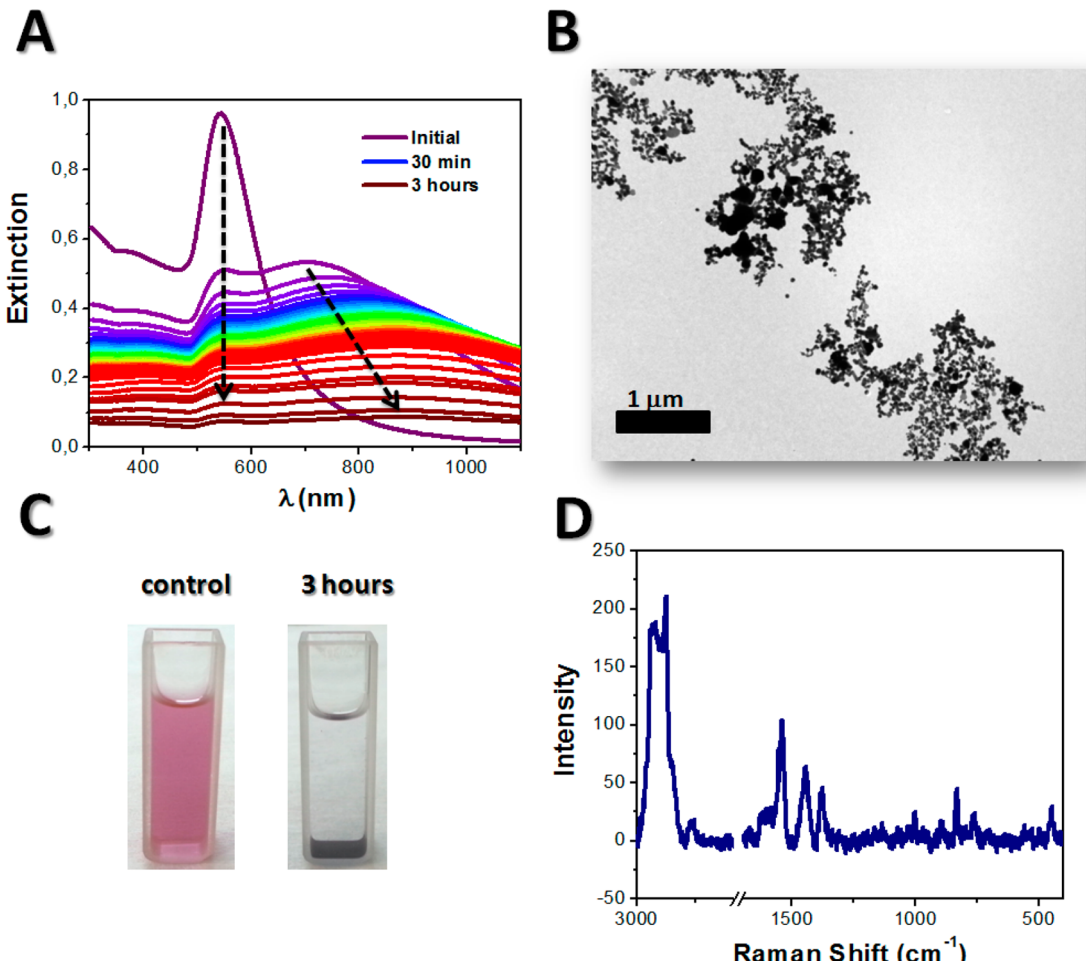


**Figure 1.** Far and Near Field Optical as Well as Morphological Characterization of NS Assemblies Generated with Comparable Amounts of Cucurbit[6]uril Molecules and Au NSs. (A) Evolution of the extinction spectra at different times (indicated in the inset of each figure) during 76 nm Au NSs aggregation. (B) Representative TEM image of the aggregates generated after 30 min of the addition of cucurbit[6]uril ( $6.67 \times 10^{-11}$  M). (C) Real image of a cell containing the colloidal dispersion of Au NSs in the absence (left) and in the presence (right) of cucurbit[6]uril. (D) SERS spectrum irradiating the colloidal dispersion obtained after 30 min of the addition of cucurbit[6]uril.

nm.<sup>25</sup> The electron-rich carbonyl portals can interact through charge transfer with the surface of the Au NSs leading to an assembly process due to the enthalpic gain from the carbonyl-gold interactions and the entropic gain from the release of water molecules around CB[6] portals.<sup>20</sup> As mentioned before, the direct assembly of noble metal NPs with CB[n] molecules generates random aggregates whose stability depends on the final concentration of CB[n] added during the aggregation process: comparable quantities of CB[n] and NSs produce a faster aggregation process that lead to the formation of a precipitate after a few hours (2–3 h) of the addition of CB[n] (Scheme 1B), whereas the addition of a considerable excess of CB[n] leads to the formation of metastable structures due to the repulsive interactions between CB[n] molecules onto the metal surfaces (Scheme 1C).

Let us first discuss the optical behavior of random aggregates obtained by mixing comparable quantities of CB[6] and NSs. The extinction spectra and the morphological characterization of the colloidal dispersion of 76 nm Au NSs is shown in Figure S1 in the Supporting Information. Figure 1A shows the far field spectral changes at different times after the addition of CB[6] (final concentration of  $7 \times 10^{-9}$  M). The main feature to be noticed is the appearance of a second band at long wavelengths which gradually red shifts and broadens as time elapses, and

then decreases its intensity until disappears from the spectrum (no discernible plasmon excitation). This optical behavior is indicative of NS aggregation,<sup>34</sup> as it was further confirmed by TEM analysis after 30 min of reaction time (Figure 1B). As can be seen from the spectral evolution shown in Figure 1A and comparing the color of the colloidal NSs dispersion at the initial aggregation time and after 3 h of the addition of CB[6] (Figure 1C), it can be inferred that the colloidal dispersion is not stable and precipitation takes place. Even a SERS spectrum of CB[6] molecules was acquired after 30 min of reaction time (Figure 1D), this issue does not imply that these aggregates are good candidates for SERS substrates, due to the fact that the optical properties are changing dramatically during the aggregation process.<sup>34</sup> Moreover, the fact that there is no control over the number and or the geometry of the NSs in the nanostructure at each reaction time it is very difficult to use this self-assembly strategy to generate reproducible SERS substrates for quantitative sensing. This result is in agreement with previous work performed by Scherman group where they study the optical behavior during the aggregation of NPs in the presence of small quantities of CB[5], CB[7], and CB[8].<sup>21–23</sup>

As mentioned before, an excess of CB[n] molecules could lead to the formation of smaller and more stable aggregates than those generated in the aggregation process described (i.e.,

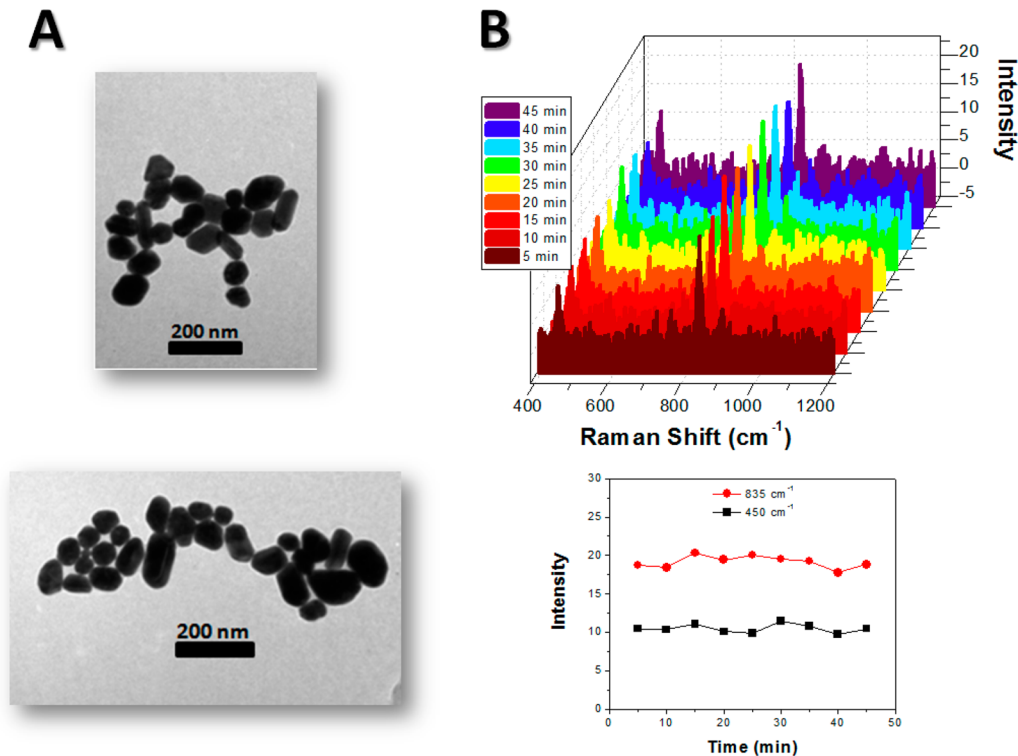
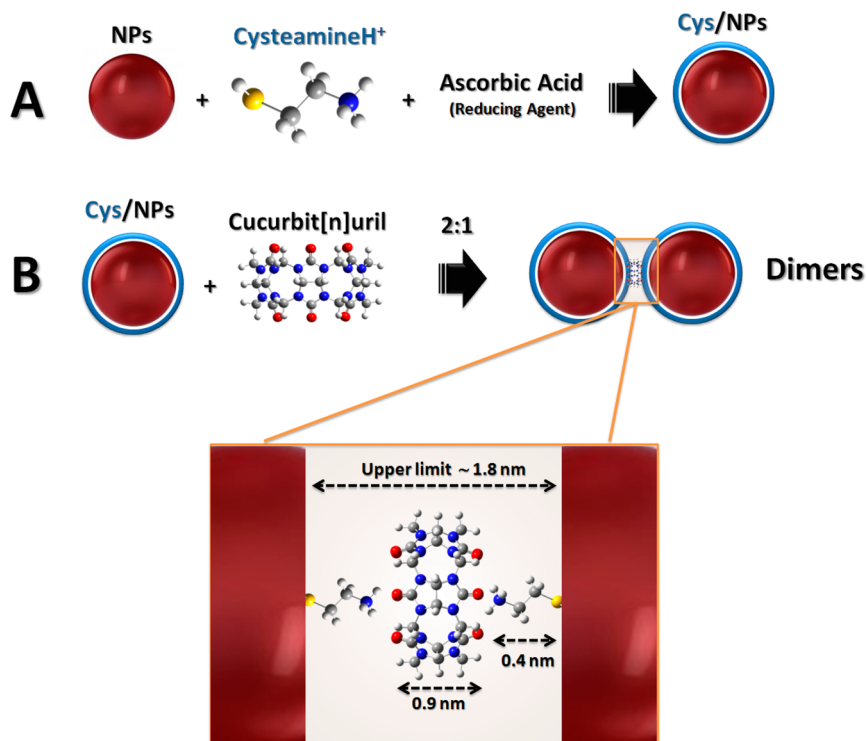


**Figure 2.** Near field optical properties and morphological characterization of NSs assemblies generated with an excess of cucurbit[6]uril molecules. (A) Two representative TEM images obtained after 30 min of the addition of cucurbit[6]uril ( $9.02 \times 10^{-7}$  M). (B) Evolution of the SERS spectra of cucurbit[6]uril during the aggregation (upper panel), and variation of the intensity of two different Raman modes of the cucurbit[6]uril indicated in the inset of the figure (lower panel).

**Scheme 2. Synthetic Scheme Showing the Nanogap Engineering for the Generation of Au Nanoparticle Dimers Using Cucurbit[n]uril Molecules<sup>a</sup>**



<sup>a</sup>(A) Nanoparticle surface functionalization with cysteamine molecules (Cys/NPs). (B) Directional assembly of functionalized Au NPs with cucurbit[n]uril, leading to dimeric structures with a 1.8 nm interparticle distance. The preferential formation of dimers depends on the molar ratio chosen between CB[n] and Cys/NPs (molar ratio 0.5:1).

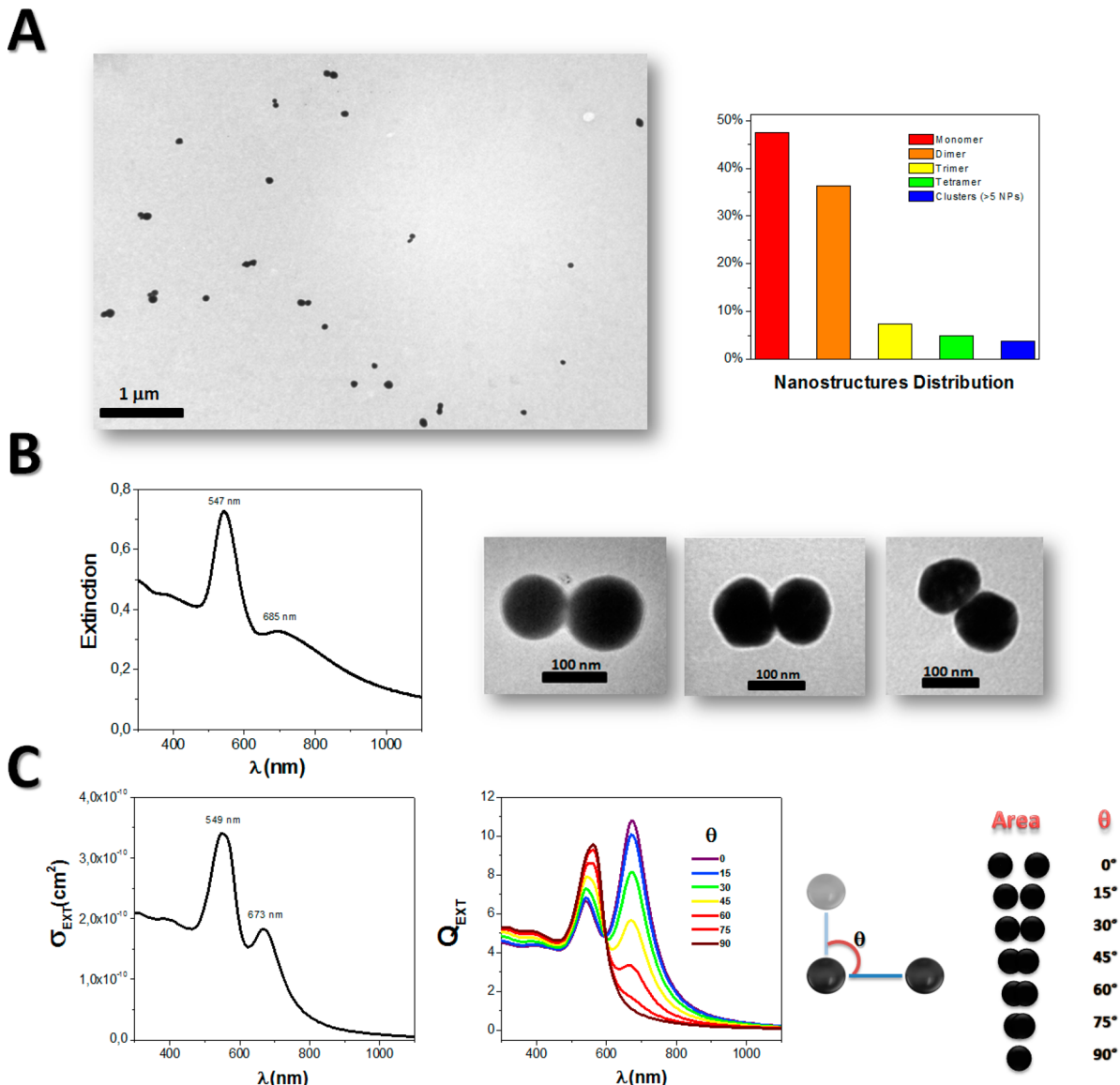


**Figure 3.** Optical and morphological characterization of 76 nm Au NS cucurbit[6]uril-linked dimers. (A) Representative wide field TEM image showing the preferential formation of dimers and the histogram of the nanostructure distribution (it is shown the percentage distribution over the 400 nanostructures). (B) Experimental extinction of the NS dimers obtained after 30 min of the addition of CB[6] (left panel), and representative TEM images of the dimers generated (right panel). (C) Average extinction cross section of the dimers (left panel), and extinction efficiency of the NS dimer at different orientations (averaged over 8 different orientations). Simulations of the 76 nm Au NS dimer with a 1.8 nm gap were performed using GMM.

the higher concentration of CB[n] completely surrounds the Au NSs, making them dispersed). The formation of smaller aggregates can be appreciated by comparing the TEM images of the NS aggregates generated by CB[6] (final concentration of  $7 \times 10^{-6}$  M) after 30 min of reaction time (Figure 2A) with the TEM image of NS aggregates generated with comparable quantities of CB[6] and NSs (See Figure 1B). The evolution of the CB[6] SERS spectra during Au NSs aggregation is shown in Figure 2B. As can be seen, the intensity of the SERS signals remains almost constant at least for 45 min, time enough to perform SERS quantitative analyses. Nevertheless, as will be discussed below, the SERS enhancements produced is lower than in more controlled nanostructures (i.e., NP dimers). This result is in agreement with previous work performed by Scherman group, where they study the formation of dynamic aggregates of NPs in the presence of an excess of CB[5].<sup>20</sup>

**Formation of Cucurbit[6]uril Self-Assembled NS Dimers.** As it has been already stated, CB[n] are rigid barrel-shaped molecules with host–guest interactions that allows one to localize the analyte molecule within the hot spot, in subnanometer gaps. These properties make this molecule a good candidate to be used as NP linker to generate ultrasensitive SERS substrates. Nevertheless, despite the number of studies that have been performed with this molecule, stable SERS substrates with controlled hot spots have not been obtained yet, which are the desirable requirements in the development of ultrasensitive quantitative SERS nanosensors. The main reason for this is that the weak interactions established between the carbonyl portals of the CB[n] molecules, and the metal surface of the NPs prevents the formation of nanostructures with precise control of the NSs geometry. In that sense, we propose a new strategy based in a

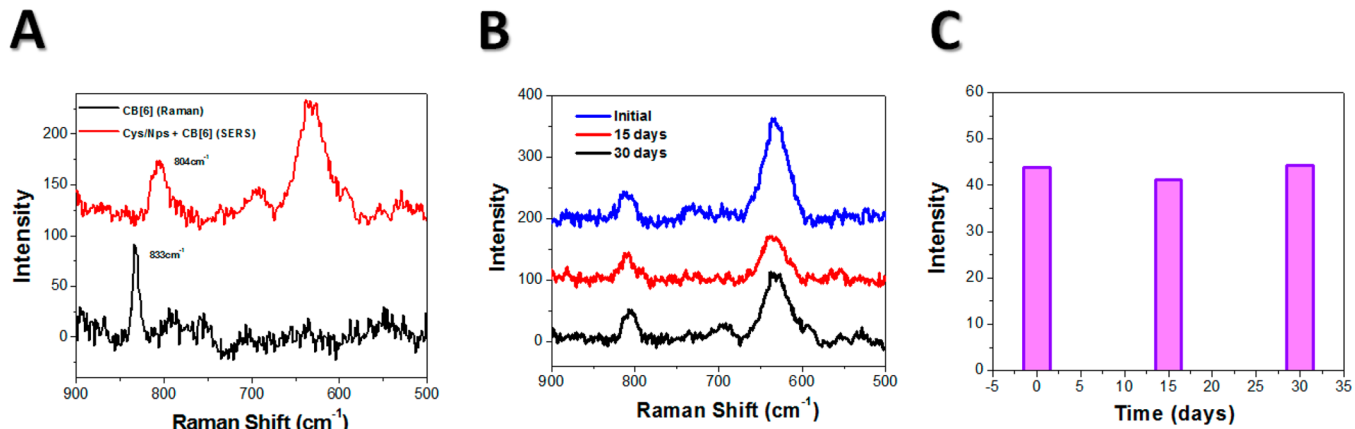


**Figure 4.** Near-field optical characterization of 76 nm Au NS dimers. (A) SERS spectra for colloidal dispersion of dimers ( $\text{CB}[6] = 6.67 \times 10^{-11}$  M) and the reference Raman spectrum of a 10 mM solution of CB[6]. (B) Stability and evolution of the SERS spectra of CB[6]. (C) Stability and evolution of the SERS intensity of the  $804 \text{ cm}^{-1}$  CB[6] vibrational mode.

previous surface modification of the NP with a capping agent that can establish strong interactions with the CB[n] molecule and, therefore, can be used to induce a more directional assembly. The high-yield synthetic strategy to obtain homodimers consists in the modification of the metal surface with cysteamine molecules (Cys) previous incubation with CB[6] (Scheme 2A). The surface modification is carried out in the presence of a reducing agent (ascorbic acid) that breaks the disulfide bonds that could be established between Cys molecules, accelerating the capping process. The cysteamine-functionalized NSs (Cys/NSs) are positive charged due to the protonation of the amine groups of the Cys molecule at the working pH (pH = 6–7). This positive group interacts through H-bonds with the carbonyl groups at the portal of de CB[6] molecules. Using a stoichiometric control over the number of Cys/NPs and CB[6] (ratio 2:1), Au NP homodimers were successfully synthesized in a relatively high yield, generating a gap of 1.8 nm, which allows to obtain reproducible hot spots (Scheme 2B).

The stability of the Au NSs colloidal dispersion was tested separately in the presence of ascorbic acid and Cys (Figures S2A and S2B, respectively). As can be seen in the figure, the spectral evolution does not depict the presence of a secondary band with respect to the plasmon resonance band of isolated Au NSs. The spectral evolution of the colloidal dispersion of Cys/NPs after the addition of CB[6] is added is presented in Figure S2C of the Supporting Information. Measurements of the average zeta potential before ( $\zeta = -19 \text{ mV}$ ) and after the functionalization with Cys ( $\zeta = +11 \text{ mV}$ ) confirms the NSs surface modification with this molecule. It is important to note that the positive potential zeta is relatively low and would only generate a moderate level of colloidal stability. Nevertheless, the presence of a secondary band in the extinction spectrum appears only when CB[6] is added in a final concentration of  $6.65 \times 10^{-11}$  M (ratio Cys/NPs and CB[6] 2:1), that is, the NP functionalization with Cys does not produce any aggregation process itself. In addition, no aggregation process was evidenced by monitoring the UV-vis spectrum after the addition of cysteamine to citrate-capped Au NSs in the range of concentration from  $1 \times 10^{-10}$  M to  $1 \times 10^{-4}$  M for several days.

Transmission electron microscopy (TEM) was undertaken on samples after 30 min of the addition of CB[6]. Conventional TEM analysis yielded a high number of dimeric nanostructures as can be appreciated in Figure 3A. The

statistics about the contribution of different assembled nanoparticles performed through the analysis of more than 400 nanostructures in the TEM images reveal that the preferential nanostructures obtained are mostly dimers (38%) together with monomers, but the presence of larger aggregates is almost negligible. The far-field spectrum obtained after 30 min of the addition of CB[6] is shown in Figure 3B. The appearance of a second band at longer wavelengths is indicative of the presence of linked NSs as a consequence of the plasmon coupling. In the present case, the aggregates formed are NS dimers as it was further confirmed by TEM analysis. Another conclusive evidence of the preferential dimer formation was obtained by the correlation between electrodynamic theory and experiments. The theoretical extinction spectrum (simulated extinction cross section,  $\sigma_{\text{EXT}}$ ) of a 76 nm Au NSs dimer with a 1.8 nm gap between particles is shown in Figure 3C. Note that the dimers are in a colloidal dispersion with a random incident polarization. According to this, the theoretical spectrum was calculated by averaging the simulated extinction efficiency ( $Q_{\text{EXT}}$ ) spectrum as a function of the angle between the dimer axis and the poynitng vector of the incident radiation ( $\theta$ ) and considering the effective geometrical area projected at each angle. The presence of a more broadened secondary band in the experiments in comparison with the simulated spectrum could be due to a noncomplete monodispersity of the NSs synthesized and also to the presence of small amounts of larger aggregates.

**Near-Field Optical Characterization and Sensing Performance of Cucurbit[6]uril Self-Assembled NS Dimers.** The synthetic approach outlined above generates NS dimers, which are a reasonably simple structure with a rigid and constant interparticle distance. As it is well-known the molecules in such nanogaps should experience an intense electromagnetic field enhancement confined within the gap (hot spot), responsible for the SERS effect. Since CB[6] is Raman-active<sup>19</sup> and is located within the gap, where the hot spots have the maximum enhancement values, these dimers are self-calibrated SERS substrates. This is so because the intensity of the SERS signals from CB[6] can be used to determine the magnitude of the maximum SERS enhancement that could be achieved. The intensity of the SERS signal at  $814 \text{ cm}^{-1}$  and the intensity of the Raman signal at  $833 \text{ cm}^{-1}$ , corresponding to the same vibrational mode of the CB[6] molecule (N–C–N deformation and CH<sub>2</sub> rocking mode), are both comparable in

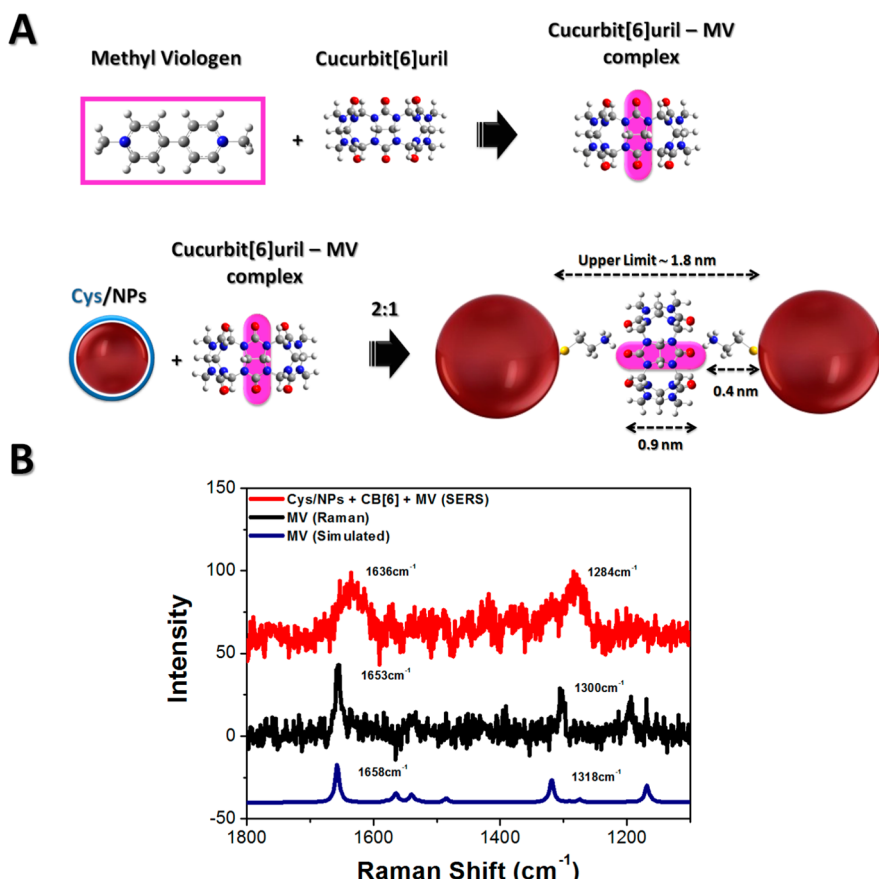


**Figure 5.** Host–guest SERS sensing properties of 76 nm Au NS cucurbit[6]uril-linked dimers. (A) Schematic representation of the inclusion of methyl viologen (MV) in the hydrophobic cavity of CB[6], and the overall experimental strategy for the SERS quantification of MV. (B) SERS spectra of a 10 pM solution of MV in the presence of cucurbit[6]uril-linked dimers (red line), reference Raman spectrum of a 1 mM solution of MV (black line), and ab initio quantum mechanics calculations of the Raman spectra of MV (blue line).

magnitude despite the difference in concentrations used to obtain the spectra were  $1.35 \times 10^{-2}$  M for CB[6] and  $6.67 \times 10^{-11}$  M for CB[6] in the colloidal dispersion (Figure 4A). Moreover, the SERS intensity corresponding to this vibrational mode remains almost constant over 30 days (Figure 4B,C). The unprecedented intensity, stability, and reproducibility of the SERS signals obtained with these nanostructures represent the central improvement of the functionalization strategy over previous works performed with CB[n] molecule as linker of plasmonic NPs. The other vibrational mode in the SERS spectra at  $630\text{ cm}^{-1}$  corresponds to the Cys molecule and it will not be considered in the analysis. The SERS spectrum of the dimers colloidal dispersion acquired in the complete fingerprint region ( $800\text{ cm}^{-1}$  to  $1800\text{ cm}^{-1}$ ) is available in the Supporting Information (Figure S3A), where it is shown that the SERS signals detected correspond to the contributions of CB[6] and Cys, as can be seen comparing the experimental SERS spectrum with the Raman spectrum of Cys and with the calculated spectrum using quantum mechanics (see Supporting Information, Figure S3A,B). Although the SERS signals of Cys could be a limiting factor for sensing applications because they could slightly overlap with the signals of a potential analyte molecule, this should be demonstrated to introduce no difficulty. As it will be discussed below, the reproducibility and stability of the dimeric substrates allow us to perform a suitable signal processing to obtain the SERS signals of only the analyte molecules.

To explain the difference in the SERS and Raman signals of the vibrational modes of CB[6] molecule it must be noted that in spectroscopy exist two main sources of broadening of peaks: a homogeneous broadening that has its origin in intramolecular anharmonic interactions and is a fundamental property of a vibration of an isolated molecule and an inhomogeneous broadening that is representative of a population of molecules and their inevitable variabilities at different places in the sample.<sup>43</sup> Hence, inhomogeneous broadenings are due to either intermolecular interactions or slightly varying interactions on a substrate, as surface interactions can introduce small perturbations in the electronic structure of adsorbed molecules. On the other hand, the homogeneous broadening is ultimately related to the anharmonic interactions that play a fundamental role in the relaxation pathways of vibrations toward equilibrium, that is, on how the energy is distributed over time once a vibration has been excited. Intrinsic anharmonic interactions tend to dominate the relaxation pathways of vibrations for many molecules, but interactions with the substrate can provide additional pathways that dominate the relaxation in other cases. The temperature dependence of the homogeneous width of a Raman mode provides information on the anharmonic coupling of that particular mode with the rest of the vibrations and the substrate.<sup>43</sup> Since metallic NPs are very inefficient light emitters, almost all energy absorbed turns into heat.<sup>44</sup> In that sense, the broaden SERS signal compared with the corresponding Raman signal (both SERS and Raman, corresponding to the N–C–N deformation and CH<sub>2</sub> rocking mode of the CB[6]

**Table 1.** Experimental Enhancement Factors for Cucurbit[6]uril Self-Assembled Random Aggregates and Dimers<sup>a</sup>

composition	c/ω (nm)	analyte	C <sub>analyte</sub> (M)	intensity (counts)	ν (cm <sup>-1</sup> )	AEF
CB[6]	633	CB[6]	1.35 × 10 <sup>-2</sup>	82	833	
CB[6] + Au NSs	633	CB[6]	9.02 × 10 <sup>-7</sup>	20	835	(3.0 ± 0.2) × 10 <sup>3</sup>
CB[6] + Cys/Au NSs	633	CB[6]	6.67 × 10 <sup>-11</sup>	56	814	(1.0 ± 0.2) × 10 <sup>8</sup>

<sup>a</sup>CB[6] = cucurbit[6]uril; Cys/Au NSs = cysteamine functionalized Au NSs; AEF = analytic enhancement factor.

molecule shown in Figure 4A) could be attributed mainly to the heating effects accompanying the LSPR excitation when the NPs are irradiated, which can affect the vibrational modes from the molecules located in the gaps of the NP dimers, and in a certain degree to the small perturbations introduced by surface interactions in the electronic structure of adsorbed molecules.

So far, we have demonstrated the potential of these dimeric nanostructures as useful SERS devices for analytical assays. Quite important, the CB[6] highly rigid and symmetric cavity with a hydrophobic inner cavity acts as a potential inclusion site for supramolecular host–guest interactions in the region of maximum field enhancement of the dimers. Going a step further, we will now test the performance of these dimeric structures to sense paraquat (1,1'-dimethyl-4,4'-dipyridinium), also known as methyl viologen (MV). We have chosen this molecule because it is a broad-spectrum herbicide that is toxic to humans and may cause acute poisoning and even deaths when ingested in high doses, and it is also known to cause diseases of the liver, lung, and heart.<sup>45–48</sup> Despite these shortcomings, MV has many advantageous agrochemical properties unrivaled by any other, making it one of the most widely used herbicides: it is a relatively nonselective, contact herbicide that is rapidly inactivated on contact with most types of soil.<sup>45,48</sup> Hence, no biologically active residues remain in the soil and planting and sowing can be carried out almost immediately after spraying.<sup>45,49</sup> Due to its widespread use, various techniques have been described for the determination of MV: spectrophotometry, chromatography, polarography, and radioimmunoassay.<sup>50</sup> These analytical methods are rather slow because of the need for extensive sample pretreatment. For this reason, they have been replaced by potentiometric sensors with detection limits around 10<sup>-6</sup> M.<sup>51</sup> Recent advances using the host–guest properties of cucurbit[8]uril for the fluorescence detection of MV has increased the detection limit to around 10<sup>-10</sup> M.<sup>52</sup> Nevertheless, fluorescence methods do not give enough spectroscopic information for the chemical identification of the guest molecule. In contrast, SERS techniques provide fingerprints of the vibrational modes of the molecules located in the hot spots, whose frequencies and relative intensities are intrinsic to the specific analyte to be identified. For this reason, some efforts have been devoted recently for the SERS detection of MV using Ag NP random aggregates generated using KNO<sub>3</sub>, but the detection limits achieved so far are significantly lower than those obtained by fluorescence techniques.<sup>53</sup> This poor SERS performance is probably due to the lack of control on the geometry design of the plasmonic substrate. The limitations of conventional techniques together with the simple sample processing and the superior sensibility of SERS methods motivated us to test the sensing capabilities of our dimeric nanostructures.

The experimental SERS spectrum of a dimer colloidal dispersion containing MV is shown in Figure S4 of the Supporting Information. These dimers were generated by previous reaction of MV (final concentration of 1 × 10<sup>-11</sup> M) with CB[6]. The SERS spectrum in the absence of MV is

shown also for comparison. The signal processing obtained by direct subtraction of the spectra of Figure S4 is shown in Figure 5. The intensity of the SERS signal at 1636 cm<sup>-1</sup> and the Raman signal at 1653 cm<sup>-1</sup>, both corresponding to the same vibrational mode of the MV molecule (C=C stretching and CH<sub>3</sub> bending), as well as the intensity of the SERS signal at 1284 cm<sup>-1</sup> and the intensity of the Raman signal at 1300 cm<sup>-1</sup>, both corresponding to the same vibrational mode of the MV molecule (ring breathing and C–C stretching), are comparable in magnitude despite the difference in concentrations used to obtain the spectra were 1.65 × 10<sup>-3</sup> M for MV and 1.00 × 10<sup>-11</sup> M for MV in the colloidal dispersion. A further corroboration that these modes indeed corresponds to the MV molecule is evident by the close agreement between the experimental SERS spectrum, the Raman spectrum of MV and the calculated spectrum obtained with quantum mechanics.

A quantitative assessment of the near field optical properties can be obtained by a direct comparison with the SERS experimental and theoretical enhancements. The SERS enhancement factor, for many applications, is related to the simple question of how much stronger is the SERS signal produced by an analyte at a given normal mode compared to the normal Raman signal of this mode in a given experimental condition. For analytical chemistry applications, especially those involving substrates in solution, it is correct to use the analytical enhancement factor (AEF), which is defined as the ratio of the intensity of the SERS signal ( $I_{\text{SERS}}$ ) of a given mode and the intensity of the Raman signal ( $I_{\text{SR}}$ ) of the same mode for a given analyte, both normalized with the respective analyte concentration (C):<sup>54</sup>

$$\text{AEF} = \frac{I_{\text{SERS}}/C_{\text{SERS}}}{I_{\text{SR}}/C_{\text{SR}}} \quad (1)$$

This is valid as long as the experimental conditions for measuring the Raman spectrum and SERS spectrum are the same (wavelength and power of the laser, microscope objective or lens, spectrometer, etc.).

The great difference in the SERS response of our synthetic procedure to generate mostly dimeric nanostructures with CB[6] compared with the pseudostable random aggregates produced using a much higher concentration of CB[6] (see Scheme 1C and 2B, respectively) can be appreciated by comparing the AEF obtained in each case (Table 1). As can be seen, the AEF value is very low (around 10<sup>3</sup>), being below reported AEF obtained for external analytes in colloidal dispersion having more complex synthetic and irreproducible performance (10<sup>5</sup>).<sup>54,55</sup> An extraordinary improvement (from 10<sup>3</sup> to 10<sup>8</sup>) on the SERS enhancement is achieved using our synthetic approach to generate the nanostructures.

From the theoretical point of view, the main mechanism that produces the SERS effect is the electromagnetic one. Therefore, the enhancements of the SERS signals are proportional to the so-called “electromagnetic field enhancement factor”, EFEF, given by

**Table 2.** Experimental and Theoretical Enhancement Factors for Ultrasensitive SERS Plasmonic Dimers with Supramolecular Host–Guest Interactions<sup>a</sup>

composition	$c/\omega$ (nm)	analyte	$C_{\text{analyte}}$ (M)	intensity (counts)	$\nu$ (cm <sup>-1</sup> )	AEF	$c/\omega'$ (nm)	EFEFdimer <sub>max</sub>	EFEFdimer <sub>AV</sub>
CB[6]	633	CB[6]	$1.35 \times 10^{-2}$	82	833				
CB[6] + Cys/Au NSs	633	CB[6]	$6.67 \times 10^{-11}$	56	814	$(1.0 \pm 0.2) \times 10^8$	696	$2.6 \times 10^9$	$2.4 \times 10^8$
MV	633	MV	$1.65 \times 10^{-3}$	39	1653				
MV + CB[6] + Cys/Au NSs	633	MV	$1.00 \times 10^{-11}$	36	1636	$(1.0 \pm 0.3) \times 10^8$	686	$2.6 \times 10^9$	$2.4 \times 10^8$

<sup>a</sup>CB[6] = cucurbit[6]uril; Cys/Au NSs = cysteamine functionalized Au NSs; MV = methyl viologen; AEF = analytic enhancement factor; EFEFdimer<sub>MAX</sub> = theoretical electromagnetic field enhancement factor considering only the maximum enhancement. EFEFdimer<sub>AV</sub> = theoretical electromagnetic field enhancement factor averaged over 8 different polarizations and considering  $\Gamma \geq 100$ .

$$\text{EFEF} = |\Gamma(\omega)| |\Gamma(\omega')| \quad (2)$$

$$|\Gamma(\omega)| = \left( \left| \frac{E(\omega)}{E_0(\omega)} \right| \right)^2 \quad (3)$$

$$|\Gamma(\omega')| = \left( \left| \frac{E(\omega')}{E_0(\omega')} \right| \right)^2 \quad (4)$$

where  $|\Gamma(\omega)|$  is the square of the enhanced electric field generated at the frequency of the incident radiation ( $\omega$ ) and  $|\Gamma(\omega')|$  is the square of the enhanced electric field generated at a particular Stokes frequency ( $\omega'$ ).<sup>56</sup> For a more realistic comparison with the experiments, the EFEF has been computed using different lower limits of the enhancement ( $\Gamma_{\min}$ ) to perform the integration:

$$\left\langle \Gamma(\omega) \right\rangle_{\theta}^{\Gamma_{\min}} = \int_{\Gamma_{\min}}^{\Gamma_{\max}} \Gamma_i(\omega) d\omega / \int_{\Gamma_{\min}}^{\Gamma_{\max}} d\omega \quad (5)$$

where  $i$  corresponds to the  $i$ th point in the grid simulated, and  $\theta$  corresponds to the angle between the dimer axis and the poynting vector of the incident radiation. As it should be expected, increasing the lower limit of integration ( $\Gamma_{\min}$ ), the larger is the value of EFEF. Notwithstanding, the regions of highest enhancement are achieved in the hot spots between closely interacting NPs with an effective area occupied by the CB[n] molecule. Therefore, the experimental SERS signals can not only be attributed to the small region of maximum enhancement generated in the gaps (i.e., this only occurs in a single point of the simulation grid). A more suitable procedure is to calculate the average enhancement corresponding to the area occupied by the analyte molecule. This average enhancement will strongly depend on the lower limit of the enhancement ( $\Gamma_{\min}$ ) used to perform the integration in eq 5. Regions with  $\Gamma \geq 9$  overestimate the effective area of the CB[6] molecule, while regions with  $\Gamma \geq 400$  considers only the small region of maximum enhancement. After several trials, we have determined that the region with enhancements  $\Gamma \geq 100$  generates a hot spot with a size comparable with the molecule area (1.62 nm<sup>2</sup>). Another issue that should be accounted for is the fact that the dimers are in a colloidal dispersion with a random incident polarization. Therefore, the EFEF should be averaged over different angles between the dimer axis and the poynting vector of the incident radiation.

Using these definitions, the EFEF calculated according to eq 2 will be compared with the AEF given by eq 1 for dimers synthesized. There is an excellent correlation between the AEF and the EFEF ( $10^8$ ), calculated for the selected modes of CB[6] (Table 2). These values are within the maximum AEF

values for SERS substrates in solution.<sup>13,57</sup> The theoretical maximum enhancement (considering the point of maximum enhancement in the simulated grid) of the dimers is a factor of 10 greater than the experimental AEF. This could be considered as an upper bound to the experimental enhancement observed. A more correct comparison with the experiments is achieved calculating the EFEF considering eq 5, which takes into account the effective area of the molecule. Table 2 also shows the results of the AEF for the SERS detection of MV using the dimers as nanosensors, together with the EFEF of the Au NS dimer. The excellent correlation between the experimental AEF of the MV molecule with the experimental AEF of the CB[6] and the EFEF of the dimer, all being around  $10^8$ , indicates that the detection of MV is achieved due to the molecules inside the cavity of CB[6]. Note also that the fact that the AEF of de dimers in the absence and in the presence of MV are almost the same suggests that there is not any significant change in the interparticle distance due to the presence of a guest molecule inside the CB[6] host. This feature was also checked by comparing the far field spectrum of the dimers colloidal dispersion in presence and absence of MV (see Figure S5 of the Supporting Information), as in both cases the position of the dimer longitudinal plasmon resonance is at the same wavelength.

According to our theoretical EFEF calculation, the already significant SERS enhancement achieved could be further improved by irradiating at 684 nm (see Figure S6 of the Supporting Information, where a comparison of the extinction spectrum and the simulated near field enhancement spectrum of a NS dimer is presented). Nevertheless, using the experimental available laser at 633 nm, the enhancement is still quite high (only a factor 4–10 smaller than the optimum one).

Finally, even the SERS signals of the Cys molecule could make difficult the detection of analyte molecules, we demonstrate that a very simple signal processing allow us to detect an analyte molecule (in this case we detect MV as a concept probe). Note that as the signal/noise for the MV spectrum is weak, the detection of this molecule in a real sample where other small molecules could form inclusion complexes with CB[6] could affect the detection sensitivity. The weak signal/noise obtained is related to the SERS signals of Cys because they overlap with the signals of MV. Nevertheless, there is an “open window” in the 1100 and 800 cm<sup>-1</sup> range in the SERS spectrum of the dimeric colloidal dispersion that is free of these sensing limitations. This feature make these substrates excellent candidates for the detection of many polycyclic aromatic hydrocarbons (PAHs), since these molecules have very strong and characteristic signals around 1000 cm<sup>-1</sup> (ring breathing modes). This feature make this

substrates excellent candidates for the detection of many polycyclic aromatic hydrocarbons (PAHs), since these molecules have very strong and characteristic signals around  $1000\text{ cm}^{-1}$  (ring breathing modes). The interest in PAHs is because they are a class of pollutants that need to be monitored at ultralow concentrations, therefore requiring long sampling times and preconcentration to obtain measurable signals using the conventional methods mentioned before. The interest in PAHs is because they are a class of pollutants that need to be monitored at ultralow concentrations, therefore, requiring long sampling times and preconcentration to obtain measurable signals using the conventional methods mentioned before. In the case of CB[6], the small portal only allows small molecules to interact with the hydrophobic nanocavity. In that sense, previous studies show that CB[6] can form complexes with pyrene (PYR),<sup>25</sup> which is representative of PAHs, as stated in the Scientific Opinion of the Panel on Contaminants in the Food Chain: Pyrene is present in all PAH mixtures at relatively high concentrations (2–10% of the total PAHs). In addition, previous works show the potential of using the supramolecular host–guest interactions of the hydrophobic cavity of CB[8] to characterize these organic molecules.<sup>23</sup> The synthetic strategy shown in this work could be easily applied with other CB[n] homologues, which can be used as host for these molecules, in particular, CB[8], without any significant change of the extraordinary sensitivity and SERS enhancement of the dimeric substrates analyzed in this work. Research in this direction is under development and will be the subject of future work.

## CONCLUSIONS

The central contribution of the present work is the development of a reproducible synthetic strategy to obtain stable plasmonic dimeric nanostructures that give rise to high SERS enhancements. The dimeric nanostructures retain the host–guest properties of the macrocycle, with the potential capability of detecting analytes at picomolar concentrations. In that sense, self-calibrated SERS dimeric Au nanostructures have been successfully prepared in a reproducible way using cucurbit[6]-uril (CB[6]) as linker. The stability of these colloidal dispersions, together with the rigorous control of the interparticle distance between NSs (gap = 1.8 nm), allow us to generate nanostructures with reproducible hot spots. The novel synthetic strategy is based on a strict stoichiometric control between CB[6] and cys-functionalized NSs (Cys/NSs). We have shown that strong and reproducible SERS signals, with enhancement factors around  $10^8$ , can be obtained for these dimeric substrates for the CB[6] molecule acting as a SERS reporter. These sensors are self-calibrated in the sense that whenever a dimer has been synthesized, a rough determination of the SERS enhancement allows us to estimate the maximum enhancement that could be achieved. In addition, the capability of these dimeric substrates for detecting a specific analyte molecule is demonstrated by placing the analyte within the gap junctions using the host–guest properties of the CB[n] molecule. In this case we identified and quantify the presence of a widely used herbicide (MV), reaching a detection limit of  $1 \times 10^{-11}\text{ M}$ , which exceeds several orders of magnitude the detection limits previously reported.

The excellent agreement between modeling and experiments allowed us to explain the very rich near and far field plasmonic behavior of these dimers, indicating that the geometry and the interparticle distance assumed for the dimers is correct. Moreover, the simulation of the near field response of these

dimeric structures allows us to explain the differences in the AEF, in terms of angular average and the effective area of the enhancement.

## ASSOCIATED CONTENT

### S Supporting Information

Optical and morphological characterization of Au NSs; Optical characterization of the functionalization process of Cys/Au NSs and the formation of CB[6]-linked dimers; SERS optical characterization of 76 nm Au NSs CB[6]-linked dimers; SERS optical characterization of the host–guest properties of CB[6]-linked Au NS dimers; Far field optical characterization of the host–guest properties of CB[6]-linked Au NS dimers; Near field optical characterization of 76 nm Au NSs CB[6]-linked dimers. This material is available free of charge via the Internet at <http://pubs.acs.org>.

## AUTHOR INFORMATION

### Corresponding Author

\*E-mail: coronado@fcq.unc.edu.ar.

### Notes

The authors declare no competing financial interest.

## ACKNOWLEDGMENTS

Authors also acknowledge financial support of CONICET (PIP 112-201101-00430 and PIP 112-200901-00843), FONCYT (PICT 2012-2286), SECYT-UNC, and PME 1544–2006. J.C.F. acknowledges CONICET for being recipient of a Ph.D. fellowship. We thank Dr. R. H. de Rossi for her valuable suggestions and encouragement.

## REFERENCES

- (1) Kelly, K. L.; Coronado, E. A.; Zhao, L. L.; Schatz, G. C. The Optical Properties of Metal Nanoparticles: The Influence of Size, Shape, and Dielectric Environment. *J. Phys. Chem. B* **2003**, *107*, 668–677.
- (2) Halas, N. J.; Lal, S.; Chang, W.-S.; Link, S.; Nordlander, P. Plasmons in Strongly Coupled Metallic Nanostructures. *Chem. Rev.* **2011**, *111*, 3913–3961.
- (3) Marhaba, S.; Bachelier, G.; Bonnet, C.; Broyer, M.; Cottancin, E.; Grillet, N.; Lermé, J.; Vialle, J.-L.; Pellarin, M. Surface Plasmon Resonance of Single Gold Nanodimers Near the Conductive Contact Limit. *J. Phys. Chem. C* **2009**, *113*, 4349–4356.
- (4) Kambhampati, P.; Child, C. M.; Foster, M. C.; Campion, A. On the Chemical Mechanism of Surface Enhanced Raman Scattering: Experiment and Theory. *J. Chem. Phys.* **1998**, *108*, 5013–5026.
- (5) Su, K. H.; Wei, Q. H.; Zhang, X.; Mock, J. J.; Smith, D. R.; Schultz, S. Interparticle Coupling Effects on Plasmon Resonances of Nanogold Particles. *Nano Lett.* **2003**, *3*, 1087–1090.
- (6) Jiang, J.; Bosnick, K.; Maillard, M.; Brus, L. Single Molecule Raman Spectroscopy at the Junctions of Large Ag Nanocrystals. *J. Phys. Chem. B* **2003**, *107*, 9964–9972.
- (7) Gunnarsson, L.; Bjerneld, E. J.; Xu, H.; Petronis, S.; Kasemo, B.; Kall, M. Interparticle Coupling Effects in Nanofabricated Substrates for Surface-Enhanced Raman Scattering. *Appl. Phys. Lett.* **2001**, *78*, 802–804.
- (8) Jain, P. K.; El-Sayed, M. A. Surface Plasmon Coupling and Its Universal Size Scaling in Metal Nanostructures of Complex Geometry: Elongated Particle Pairs and Nanosphere Trimers. *J. Phys. Chem. C* **2008**, *112*, 4954–4960.
- (9) Rechberger, W.; Hohenau, A.; Leitner, A.; Krenn, J. R.; Lamprecht, B.; Aussenegg, F. R. Optical Properties of Two Interacting Gold Nanoparticles. *Opt. Commun.* **2003**, *220*, 137–141.

- (10) Xu, H. X.; Aizpurua, J.; Kall, M.; Apell, P. Electromagnetic Contributions to Single-Molecule Sensitivity in Surface-Enhanced Raman Scattering. *Phys. Rev. E* **2000**, *62*, 4318–4324.
- (11) Prodan, E.; Radloff, C.; Halas, N. J.; Nordlander, P. A Hybridization Model for the Plasmon Response of Complex Nanostructures. *Science* **2003**, *302*, 419–422.
- (12) Nordlander, P.; Oubre, C.; Prodan, E.; Li, K.; Stockman, M. I. Plasmon Hybridization in Nanoparticle Dimers. *Nano Lett.* **2004**, *4*, 899–903.
- (13) Fraire, J. C.; Pérez, L. A.; Coronado, E. A. Rational Design of Plasmonic Nanostructures for Biomolecular Detection: Interplay between Theory and Experiments. *ACS Nano* **2012**, *6*, 3441–3452.
- (14) Fraire, J. C.; Masseroni, M. L.; Jausoro, I.; Perassi, E. M.; Diaz-Añel, A. M.; Coronado, E. A. Design of Plasmonic Probes for the Identification, Localization and Quantification of Cell Membrane Receptors: Evaluating the Role of PKD1 in the Distribution of Neuronal Glutamate Receptors. *ACS Nano* **2014**, *6*, 3441–3452.
- (15) Lee, H.; Lee, J.-H.; Jin, S. M.; Suh, Y. D.; Nam, J.-M. Single-Molecule and Single-Particle-Based Correlation Studies between Localized Surface Plasmons of Dimeric Nanostructures with ~1 nm Gap and Surface-Enhanced Raman Scattering. *Nano Lett.* **2013**, *13*, 6113–6121.
- (16) Lim, D.-K.; Jeon, K.-S.; Kim, H. M.; Nam, J.-M.; Suh, Y.-D. Nanogap-Engineerable Raman-Active Nanodumbbells for Single-Molecule Detection. *Nat. Mater.* **2010**, *9*, 60–67.
- (17) Lee, J.-H.; Nam, J.-M.; Jeon, K.-S.; Lim, D.-K.; Kim, H.; Kwon, S.; Lee, H.; Suh, Y.-D. Tuning and Maximizing the Single-Molecule Surface-Enhanced Raman Scattering from DNA-Tethered Nanodumbbells. *ACS Nano* **2012**, *6*, 9574–9584.
- (18) Yi, C.; Liu, D.; Yang, M. Building Nanoscale Architectures by Directed Synthesis and Self-Assembly. *Curr. Nanosci.* **2009**, *5*, 75–87.
- (19) Mahajan, S.; Lee, T.-C.; Biedermann, F.; Hugall, J. T.; Baumberg, J. J.; Scherman, O. A. Raman and SERS Spectroscopy of Cucurbit[n]urils. *Phys. Chem. Chem. Phys.* **2010**, *12*, 10429–10433.
- (20) Lee, T.-C.; Scherman, O. A. Formation of Dynamic Aggregates in Water by Cucurbit[5]uril Capped With Gold Nanoparticles. *Chem. Commun.* **2010**, *46*, 2438–2440.
- (21) Richard, W. T.; Lee, T.-C.; Scherman, O. A.; Esteban, R.; Aizpurua, J.; Huang, F. M.; Baumberg, J. J.; Mahajan, S. Precise Subnanometer Plasmonic Junctions for SERS within Gold Nanoparticle Assemblies Using Cucurbit[n]uril Glue. *ACS Nano* **2011**, *5*, 3878–3887.
- (22) Richard, W. T.; Esteban, R.; Mahajan, S.; Coulston, R.; Scherman, O. A.; Aizpurua, J.; Baumberg, J. J. Simple Composite Dipole Model for the Optical Modes of Strongly-Coupled Plasmonic Nanoparticle Aggregates. *J. Phys. Chem. C* **2012**, *116*, 25044–25051.
- (23) Kasera, S.; Biedermann, F.; Baumberg, J. J.; Scherman, O. A.; Mahajan, S. Quantitative SERS Using the Sequestration of Small Molecules Inside Precise Plasmonic Nanoconstructs. *Nano Lett.* **2012**, *12*, 5924–5928.
- (24) Richard, W. T.; Coulston, R. J.; Biedermann, F.; Mahajan, S.; Baumberg, J. J.; Scherman, O. A. In Situ Monitoring of Photochemistry within a Nanojunction Reactor. *Nano Lett.* **2013**, *13*, 5985–5990.
- (25) Suelo Occello, V. N.; Veglia, A. V. Cucurbit[6]uril Nanocavity as an Enhanced Spectrofluorimetric Method for the Determination of Pyrene. *Anal. Chim. Acta* **2011**, *689*, 97–102.
- (26) Day, A.; Arnold, A. P.; Blanch, R. J.; Snushall, B. Controlling Factors in the Synthesis of Cucurbituril and Its Homologues. *J. Org. Chem.* **2001**, *66*, 8094–8100.
- (27) Lagona, J.; Muckhopadhyay, P.; Chakrabarti, S.; Isaacs, L. The Cucurbit[n]uril Family. *Angew. Chem., Int. Ed.* **2005**, *44*, 4844–4870.
- (28) Jeon, W. S.; Moon, K.; Park, S. H.; Chun, H.; Ko, Y. H.; Y-Lee, J.; Lee, E. S.; Samal, S.; Selvapalam, N.; Rekharsky, M. V.; et al. Complexation of Ferrocene Derivatives by the Cucurbit[7]uril Host: A Comparative Study of the Cucurbituril and Cyclodextrin Host Families. *J. Am. Chem. Soc.* **2005**, *127*, 12984–12989.
- (29) Ong, W.; Gomez-Kaifer, M.; Kaifer, A. E. Cucurbit[7]uril: A Very Effective Host for Viologens and Their Cation Radicals. *Org. Lett.* **2002**, *4*, 1791–1794.
- (30) Eelkema, R.; Maeda, K.; Odell, B.; Anderson, H. L. Radical Cation Stabilization in a Cucurbituril Oligoaniline Rotaxane. *J. Am. Chem. Soc.* **2007**, *129*, 12384–12385.
- (31) Kasuga, N. C.; Umeda, M.; Kidokoro, H.; Ueda, K.; Hattori, K.; Yamaguchi, K. Four Novel Solid-State Supramolecular Assemblies Constructed from Decavanadate Salts and Decamethylcucurbit[5]uril. *Cryst. Growth Des.* **2009**, *9*, 1494–1498.
- (32) Rekharsky, M. V.; Yamamura, H.; Inoue, C.; Kawai, M.; Osaka, I.; Arakawa, R.; Shiba, K.; Sato, A.; Ko, Y. H.; Selvapalam, N.; et al. Chiral Recognition in Cucurbituril Cavities. *J. Am. Chem. Soc.* **2006**, *128*, 14871–14880.
- (33) Jones, S. T.; Taylor, R. W.; Esteban, R.; Abo-Hamed, E. K.; Bomans, P. H. H.; Sommerdijk, N. A. J. M.; Aizpurua, J.; Baumberg, J. J.; Scherman, O. A. Gold Nanorods with Sub-Nanometer Separation Using Cucurbit[n]uril for SERS Applications. *Small* **2014**, *10*, 4298–4303.
- (34) Fraire, J. C.; Pérez, L. A.; Coronado, E. A. Cluster Size Effects in the SERS Response of Ag and Au Nanoparticle Aggregates: Experimental and Theoretical Insight. *J. Phys. Chem. C* **2013**, *117*, 23090–23107.
- (35) Turkevich, J.; Stevenson, P. C.; Hillier, J. A Study of the Nucleation and Growth Processes in the Synthesis of Colloidal Gold. *Discuss. Faraday Soc.* **1951**, *11*, 55–75.
- (36) Freedman, W. A.; Mock, W. L.; Shih, N. Y.; Cucurbituril. *J. Am. Chem. Soc.* **1981**, *103*, 7367–7368.
- (37) Suelo Occello, V. N. *Ph.D. Thesis*, Facultad de Ciencias Químicas, Universidad Nacional de Córdoba, Córdoba, Argentina, 2011.
- (38) Encina, E. R.; Coronado, E. A. On the Far Field Optical Properties of Ag–Au Nanosphere Pairs. *J. Phys. Chem. C* **2010**, *114*, 16278–16284.
- (39) Encina, E. R.; Coronado, E. A. Plasmon Coupling in Silver Nanosphere Pairs. *J. Phys. Chem. C* **2010**, *114*, 3918–3923.
- (40) Encina, E. R.; Coronado, E. A. Near Field Enhancement in Ag–Au Nanospheres Heterodimers. *J. Phys. Chem. C* **2011**, *115*, 15908–15914.
- (41) Palik, E. D. *Handbook of Optical Constants of Solids*. Academic Press: New York, 1985.
- (42) Frisch, M. J.; Trucks, G. W.; Schlegel, H. B.; Scuseria, G. E.; Robb, M. A.; Cheeseman, J. R.; Zakrzewski, V. G.; Montgomery, J. A., Jr.; Stratmann, R. E.; Burant, J. C.; et al. *Gaussian 98*, Revision A.7; Gaussian, Inc.: Pittsburgh, PA, 1998.
- (43) Artur, C.; Le Ru, E. C.; Etchegoin, P. G. Temperature Dependence of the Homogeneous Broadening of Resonant Raman Peaks Measured by Single-Molecule Surface-Enhanced Raman Spectroscopy. *J. Phys. Chem. Lett.* **2011**, *2*, 3002–3005.
- (44) Coronado, E. A.; Encina, E. R.; Stefan, F. D. Optical Properties of Metallic Nanoparticles: Manipulating Light, Heat and Forces at the Nanoscale. *Nanoscale* **2011**, *3*, 4042–4059.
- (45) Sagar, G. R. Uses and Usefulness of Paraquat. *Hum. Toxicol.* **1987**, *6*, 7–11.
- (46) Corasaniti, M. T.; Nistico, G. Determination of Paraquat in Rat Brain by High-Performance Liquid Chromatography. *J. Chromatogr.* **1993**, *643*, 419–425.
- (47) Meredith, T. J.; Vale, J. A. Treatment of Paraquat Poisoning in Man: Methods to Prevent Absorption. *Hum. Toxicol.* **1987**, *6*, 49–55.
- (48) Braithwaite, R. A. Emergency Analysis of Paraquat in Biological Fluids. *Hum. Toxicol.* **1987**, *6*, 83–86.
- (49) Vale, J. A.; Volans, G. N. The Second European Symposium on Paraquat Poisoning, 27th January 1986, Guy's Hospital, London. *Hum. Toxicol.* **1987**, *6*, 3–86.
- (50) Vale, J. A.; Volans, G. N. Paraquat Sensors Based on Cyclotetrasiloxanes. *Anal. Chim. Acta* **1994**, *285*, 271–276.
- (51) Saad, B.; Ariffin, M. M.; Saleh, M. I. Paraquat Sensors Containing Membrane Components of High Lipophilicities'. *Anal. Chim. Acta* **1997**, *338*, 89–96.

- (52) Sun, S.; Li, F.; Liu, F.; Wang, J.; Peng, X. Fluorescence Detecting of Paraquat using Host-Guest Chemistry with Cucurbit[8]-uril. *Sci. Rep.* **2014**, *4*, 1–5.
- (53) Roldan, M. L.; Corrado, G.; Francioso, O.; Sanchez-Cortes, S. Interaction of Soil Humic Acids with Herbicide Paraquat Analyzed by Surface-Enhanced Raman Scattering and Fluorescence Spectroscopy on Silver Plasmonic Nanoparticles. *Anal. Chim. Acta* **2011**, *699*, 87–95.
- (54) Le Ru, E. C.; Blackie, E.; Meyer, M.; Etchegoin, P. G. Surface Enhanced Raman Scattering Enhancement Factors: A Comprehensive Study. *J. Phys. Chem. C* **2007**, *111*, 13794–13803.
- (55) Kang, T.; Yoon, I.; Kim, J.; Ihée, H.; Kim, B. Au Nanowire-Au Nanoparticles Conjugated System Which Provides Micrometer Size Molecular Sensors. *Chem.—Eur. J.* **2010**, *16*, 1351–1355.
- (56) Le Ru, E.; Etchegoin, P. G. *Principles of Surface Enhanced Raman Spectroscopy*; Elsevier Publishing: Amsterdam, 2009; Vol 1.
- (57) Connolly, S.; Fitzmaurice, D. Programmed Assembly of Gold Nanocrystals in Aqueous Solution. *Adv. Mater.* **1999**, *11*, 1202–1205.